# Fluorescence measurements reveal stoichiometry of $K^+$ channels formed by modulatory and delayed rectifier $\alpha$-subunits

**Daniel Kerschensteiner*†, Florentina Soto‡, and Martin Stocker*†**

*Department of Pharmacology, Wellcome Laboratory of Molecular Pharmacology, University College London, Gower Street, London WC1E 6BT, United Kingdom; and ‡Abteilung Molekulare Biologie Neuronaler Signale, Max-Planck-Institut für Experimentelle Medizin, Hermann-Rein-Strasse 3, 37075 Göttingen, Germany

Edited by Ramon Latorre, Center for Scientific Studies, Valdivia, Chile, and approved February 18, 2005 (received for review January 19, 2005)

**Modulatory $\alpha$-subunits, which comprise one-fourth of all voltage-gated $K^+$ channel (Kv) $\alpha$-subunits, do not assemble into homomeric channels, but selectively associate with delayed rectifier Kv2 subunits to form heteromeric channels of unknown stoichiometry. Their distinct expression patterns and unique functional properties have made these channels candidate molecular correlates for a broad set of native $K^+$ currents. Here, we combine FRET and electrophysiological measurements to determine the stoichiometry and geometry of heteromeric channels composed of the delayed rectifier Kv2.1 subunit and the modulatory Kv9.3 $\alpha$-subunit. Kv channel $\alpha$-subunits were fused with GFP variants, and heteromerization of different combinations of tagged and untagged $\alpha$-subunits was studied. FRET, evaluated by acceptor photobleaching, was only observed upon formation of functional channels. Our results, obtained from two independent experimental paradigms, suggest the formation of heteromeric Kv2.1/Kv9.3 channels of fixed stoichiometry consisting of three Kv2.1 subunits and one Kv9.3 subunit. Strikingly, despite this uneven stoichiometry, we find that heteromeric Kv2.1/Kv9.3 channels maintain a pseudo-symmetric arrangement of subunits around the central pore.**

FRET | voltage-gated $K^+$ channel | potassium channel | silent subunit

$K^+$ channels comprise a diverse and ubiquitous class of proteins that mediate the selective transport of $K^+$ ions across cell membranes. Among them, voltage-gated $K^+$ (Kv) channels open in response to membrane depolarization, allowing the efflux of $K^+$, which in turn, repolarizes the membrane endowing excitable cells with a negative feedback switch that terminates action potentials (1). The pathway of ions through Kv channels, the pore, is lined by four $\alpha$-subunits, with each subunit contributing equally to its formation. Kv channels open and close by different conformational changes that are referred to collectively as gating transitions. A diverse set of intracellular and transmembrane auxiliary subunits has evolved to regulate these gating transitions and tune native Kv channels to tissue-specific requirements (1). A consistent observation so far is that an even number of pore-forming $\alpha$-subunits and auxiliary subunits assemble into symmetric Kv channel complexes (2–5). Modulatory $\alpha$-subunits combine features of both auxiliary proteins and $\alpha$-subunits and comprise the largest group of mammalian $K^+$ channel-regulating proteins so far described, consisting of Kv5.1, Kv6.1–6.4, Kv8.1–8.2, and Kv9.1–9.3 subunits (6–12). When expressed in heterologous systems, modulatory $\alpha$-subunits are unable to form homomeric channels but selectively interact with delayed rectifier subunits of the Kv2 subfamily to form heteromeric channels with unique functional properties that can be correlated with a number of native channels (e.g., 12). The functional properties of some of these heteromeric channels have been described in detail (9, 12, 13), and structural determinants of the regulatory function of modulatory $\alpha$-subunits have been identified (14, 15). However, the stoichiometry and geometric arrangement of their assembly with Kv2 subunits are unknown.

To study these structural features of Kv2.1/9.3 heteromeric channels, we used FRET in combination with electrophysiological measurements in two experimental paradigms. FRET, which can be observed when appropriate acceptor and donor fluorophores are in close proximity (<10 nm) (16), has previously been successfully used to determine the stoichiometry (17) and conformational rearrangements of ion channels (18, 19). Our data suggest that Kv2.1 and Kv9.3 $\alpha$-subunits heteromerize into functional Kv channels with a fixed stoichiometry of three Kv2.1 subunits and one Kv9.3 subunit.

## Materials and Methods

**Molecular Biology.** Enhanced cyan fluorescent protein (CFP) and enhanced yellow fluorescent protein (YFP) from pCB6-CMV-CFP and pCB6-CMV-YFP were combined with Kv2.1 and Kv9.3 cDNAs from rat in pcDNA3 to generate N-terminally tagged channels. The amino acid (aa) linker regions were as follows: $_{CFP}$Kv2.1 and $_{YFP}$Kv2.1 (LYKGGRLPA), $_{CFP}$Kv9.3, and $_{YFP}$Kv9.3 (LYKGGRLVF). The underlined amino acids correspond to fluorophore and channel subunits. All constructs were verified by sequencing.

**Cell Biology.** Human embryonic kidney (HEK)293 cells were grown as described in ref. 20 and transfected by using FuGENE 6 (Roche Applied Science, Mannheim, Germany) or LipofectAMINE (Invitrogen, Karlsruhe, Germany). To study homomeric channels, 1 $\mu$g of the respective cDNA was transfected, and, for the expression of heteromeric channels, 0.5 $\mu$g of cDNA of Kv2.1, $_{CFP}$Kv2.1, or $_{YFP}$Kv2.1 was mixed with 1 $\mu$g of cDNA of Kv9.3, $_{CFP}$Kv9.3, or $_{YFP}$Kv9.3. For imaging, cells were seeded on poly-D-lysine-coated coverslips 1 day after transfection, fixed in 4% paraformaldehyde 2 days after transfection, and mounted in 100 mM Tris·HCl (pH 8.5)/25% (wt/vol) glycerol/10% (wt/vol) Molwiol 4–88 (Calbiochem, Bad Soden, Germany). For electrophysiological recordings, cells were transferred to poly-D-lysine-coated coverslips and used for up to 4 days after transfection.

**Electrophysiology.** Transiently transfected HEK293 cells were measured in the cell-attached configuration of the patch–clamp technique by using an EPC9 amplifier (HEKA, Lambrecht, Germany). Patch pipettes with tip resistances of 0.8–1.4 MΩ were pulled from Corning 0010 glass (WPI, Sarasota, FL). The

This paper was submitted directly (Track II) to the PNAS office.

Abbreviations: Kv channel, voltage-gated $K^+$ channel; CFP, cyan fluorescent protein; YFP, yellow fluorescent protein; HEK, human embryonic kidney; T1 domain, first tetramerization domain; CNG channel, cyclic nucleotide-gated channel.

†To whom correspondence may be addressed. E-mail: d.kerschensteiner@ucl.ac.uk or m.stocker@ucl.ac.uk.





www.pnas.org/cgi/doi/10.1073/pnas.0500468102

pipette solution contained 145 mM NaCl, 5 mM KCl, 3 mM $CaCl_2$, 1 mM $MgCl_2$, and 10 mM Hepes (pH 7.4). During the recording, cells were constantly perfused with 22.5 mM NaCl/140 mM KCl/2 mM $CaCl_2$/1 mM $MgCl_2$/8 mM D-Glucose/10 mM Hepes (pH 7.4). Data were acquired and analyzed with PULSE+PULSEFIT (HEKA) and IGORPRO (WaveMetrics, Lake Oswego, OR) software. Data are presented as mean ± SEM.

**Imaging Techniques.** A Zeiss LSM510 META system with a 63 × 1.25 numerical aperture oil-immersion objective was used for image acquisition. Confocal images were collected at eight-bit-intensity resolution over 512 × 512 pixels at a pixel dwell time of 12.8 μs. The 458-nm laser line was used to excite CFP and the 514-nm laser line was used to excite and bleach YFP. The spectral integrity of all constructs was confirmed before FRET experiments by using the META detector in Lambda mode. Images were obtained by using a 458- to 514-nm dichroic beamsplitter, and the META detector was set between 462.6 and 505.4 nm for CFP and between 516.1 and 601.7 nm for YFP. Under these conditions, no crosstalk was observed. FRET was measured by acceptor photobleaching, where an increase in CFP signal (dequenching) during incremental photobleaching of YFP can be observed. Background fluorescence of both fluorophores was determined from a cell-free area of the image and subtracted from the overall intensity. The mean intensity was measured from regions of interest at the outer perimeter of the cell, except for the analysis of cells expressing only modulatory α-subunits, where an intracellular region of interest was selected because no plasma membrane expression could be detected. This procedure served to restrict our analysis to fully assembled channels in the plasma membrane. Mean fluorescence intensities were measured by using IMAGEJ (National Institutes of Health) and Zeiss LSM software. FRET efficiency was calculated as:

$$E = 1 - \left(\frac{I_{DA}}{I_D}\right), \quad [1]$$

where $I_{DA}$ is the CFP-normalized fluorescence intensity before and $I_D$ is the CFP-normalized fluorescence intensity after photobleaching of the acceptor (YFP). Linear regression was used to obtain the $I_D$ values from scatter plots of the increase of CFP intensity versus the decrease of YFP intensity, with incremental photobleaching for each cell.

**Distance Computation.** FRET efficiencies from the experiments outlined in Fig. 4*A* were used to estimate the distances between adjacent and diagonally opposed subunits of heteromeric channels. For channels consisting of a single donor and three acceptor subunits, energy transfer to the diagonally opposed acceptor was assumed to be negligible (18, 21). The distance between adjacent subunits then is given by:

$$R_{adj} = R_0 \sqrt[6]{2(E^{-1} - 1)}. \quad [2]$$

Using this distance between adjacent subunits to calculate $E_{adj} = 1/[1 + R_{adj}/R_0)^6]$, the distance between subunits across the pore could then be estimated from $E = 2/3\, E_{adj} + 1/3\, E_{diag}$ for channels containing three donor subunits and one acceptor subunit according to:

$$R_{diag} = R_0 \sqrt[6]{(3E - 2E_{adj})^{-1} - 1}. \quad [3]$$

The relation between $R_{adj}$ and $R_{diag}$ was compared with that expected for a quadratic arrangement of subunits by using the Pythagorean theorem:

$$R^2_{diag} = 2R^2_{adj}. \quad [4]$$

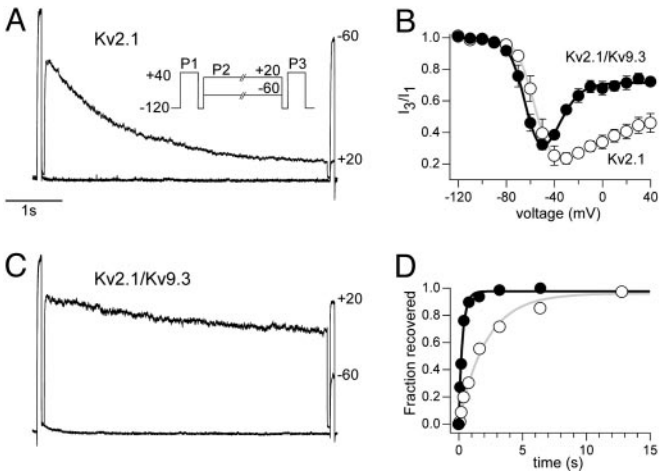


**Fig. 1.** Inactivation and recovery of Kv2.1 and Kv2.1/Kv9.3 channels. (*A*) Inactivation of Kv2.1 measured in cell-attached patches from transiently transfected HEK293 cells. Outward currents were elicited by the three-pulse protocol shown in *Inset*. Briefly, channels were inactivated during a 5-s pulse to various potentials (P2), and the degree of inactivation was determined by the ratio of currents ($I_3/I_1$) elicited by 80-ms pulses to +40 mV before (P1) and after (P3) the inactivating pulse. Representative traces are shown for P2 of −60 and +20 mV, indicative of closed- and open-state inactivation, respectively. (*B*) Inactivation of Kv2.1 (○) and Kv2.1/Kv9.3 (●) channels as a function of the potential of the inactivating pulse ($n = 6–8$). Lines represent least-square fits of the sum of two Boltzmann functions to the inactivation of Kv2.1 (gray line) and Kv2.1/Kv9.3 (black line) channels. (*C*) Representative traces of inactivation from patches of HEK293 cells transfected with Kv2.1 and Kv9.3 at a cDNA ratio of 1:2. Pulse protocol is identical to *A*. (*D*) Recovery from inactivation for Kv2.1 (○) and Kv2.1/Kv9.3 (●) channels was recorded by using a variation of the pulse protocol depicted in *A*. After maximal inactivation (P2: 10 s at −40 mV), channels were allowed to recover for increasing time intervals at the recovery potential (here −100 mV) before the fraction of channels recovered was evaluated by an 80-ms pulse to +40 mV. Solid lines represent least-square fits of monoexponential functions to the recovery of Kv2.1 (gray line) and Kv2.1/Kv9.3 (black line).

## Results

The major effects of the modulatory α-subunit Kv9.3 are illustrated by comparing inactivation and recovery of homomeric Kv2.1 and heteromeric Kv2.1/Kv9.3 channels (Fig. 1). Currents were recorded in the cell-attached configuration from HEK293 cells expressing either Kv2.1 alone (Fig. 1*A*) or both Kv2.1 and Kv9.3 (Fig. 1*C*). Inactivation was measured by using a three-pulse protocol (Fig. 1*A Inset*) where short pulses activating the channels maximally were given before and after a 5-s pulse to various potentials. Inactivation as reflected by the ratio of currents elicited by the short pulses ($I_3/I_1$) showed nonmonotonic voltage dependence for both Kv2.1 and Kv2.1/Kv9.3 channels (Fig. 1*B*). For heteromeric channels, the maximum of inactivation was shifted to hyperpolarized potentials, and reduced inactivation was observed at potentials of more than −50 mV. This biphasic voltage dependence (U shape) is thought to reflect the preference of Kv2.1 (22) and is more pronounced at Kv2.1/Kv9.3 (9) to inactivate from closed vs. open states. Recovery from inactivation of Kv2.1/Kv9.3 channels was faster (Fig. 1*D*) and less voltage-dependent (data not shown) than for Kv2.1, similar to what was observed in *Xenopus* oocytes (9). The time course of recovery in both cases was well described by a monoexponential function (Kv2.1: $\tau = 2.1 \pm 0.43$ s; Kv2.1/Kv9.3: $\tau = 0.28 \pm 0.02$ s, $n = 5$), arguing for the expression of homogenous populations of channels in the respective cells. In particular, based on these measurements, <5% of all channels in cells coexpressing Kv2.1 and Kv9.3 are expected to be homomeric Kv2.1 channels. The share of homomeric Kv2.1 channels

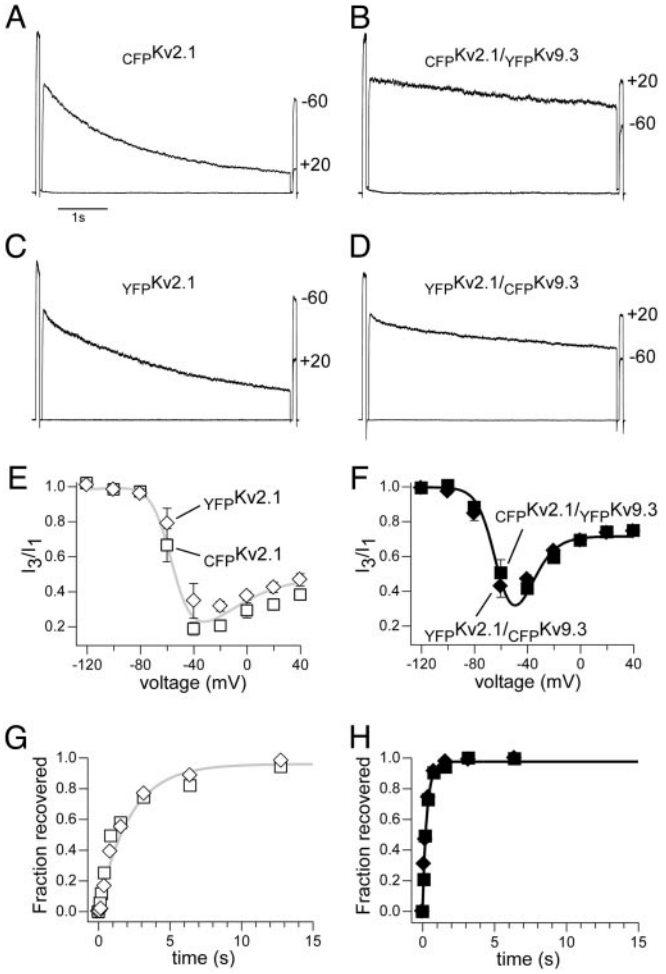


**Fig. 2.** Kinetics of fluorophore-tagged Kv2.1 and Kv2.1/Kv9.3 channels. (*A–D*) Representative scaled traces (0.8–1.6 nA amplitude), illustrating inactivation of currents recorded in cell-attached patches from HEK293 cells expressing $_{CFP}$Kv2.1 (*A*), $_{CFP}$Kv2.1/$_{YFP}$Kv9.3 (*B*), $_{YFP}$Kv2.1 (*C*), and $_{YFP}$Kv2.1/$_{CFP}$Kv9.3 (*D*). Pulse protocol is identical to the one in Fig. 1*A*. Traces are shown for P2 potentials of −60 and +20 mV. (*E–H*) $_{CFP}$Kv2.1 (□), $_{YFP}$Kv2.1 (◇), $_{CFP}$Kv2.1/$_{YFP}$Kv9.3 (■), and $_{YFP}$Kv2.1/$_{CFP}$Kv9.3 (◆). (*E* and *F*) Voltage dependence of inactivation. For comparison, the results of the voltage dependence of inactivation for untagged Kv2.1 (gray line, *E*) and Kv2.1/Kv9.3 (black line, *F*) are shown. (*G* and *H*) Recovery from inactivation measured as in Fig. 1*D*. For comparison, least-square fits of monoexponential functions describing the recovery of untagged Kv2.1 (gray line; $\tau = 2.15$ s) and Kv2.1/Kv9.3 (black line; $\tau = 0.29$ s) channels are shown.

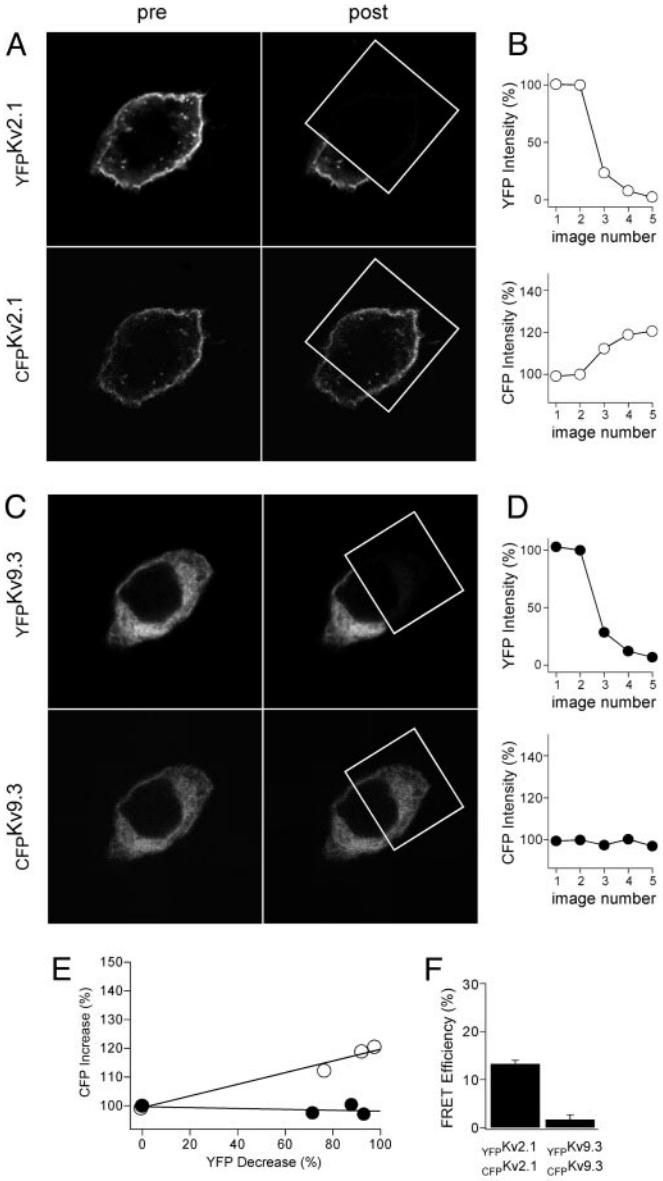


**Fig. 3.** Cellular distribution and FRET after expression of fluorophore-tagged Kv2.1 and Kv9.3 subunits. (*A*) Confocal fluorescence images of a representative cell coexpressing $_{YFP}$Kv2.1 (*Upper*) and $_{CFP}$Kv2.1 (*Lower*) before (pre) and after (post) photobleaching of the acceptor in the indicated region. (*B*) Relative fluorescence intensity measured from images taken at different times during the photobleaching of the perimeter of the cell within the region of interest indicated in *A*. (*C* and *D*) Data acquisition and analysis are analogous to *A* and *B* for a representative cell-expressing $_{YFP}$Kv9.3 and $_{CFP}$Kv9.3. The images denoted pre and post in *A* and *C* correspond to image numbers 2 and 5 in the plots, respectively. (*E*) Scatter plots of the increase of CFP and decrease of YFP fluorescence intensity during acceptor photobleaching from *B* (○) and *D* (●). (*F*) $I_D$ for complete bleaching of the acceptor was obtained by regression and used to calculate the FRET efficiency (*E*) for cells coexpressing $_{YFP}$Kv2.1 and $_{CFP}$Kv2.1 ($n = 16$) or $_{YFP}$Kv9.3 and $_{CFP}$Kv9.3 ($n = 11$).

could be increased by increasing the Kv2.1/Kv9.3 cDNA ratio. Under these conditions, the kinetics of macroscopic currents could invariably be separated into two components with identical time constants to homomeric Kv2.1 and heteromeric Kv2.1/Kv9.3 channels measured in isolation (see Fig. 5, which is published as supporting information on the PNAS web site).

To determine the stoichiometry of heteromeric Kv2.1/Kv9.3 channels by using FRET, CFP and YFP were fused to the N terminus of Kv2.1 and Kv9.3 subunits, yielding $_{CFP}$Kv2.1, $_{YFP}$Kv2.1, $_{CFP}$Kv9.3, and $_{YFP}$Kv9.3. We next verified that the CFP and YFP tags did not affect the functional properties of the resulting channels (Fig. 2), demonstrated by the superimposition of the data obtained from tagged channel subunits (data points) and untagged channel subunits (continuous lines, Fig. 2 *E–H*). Accordingly, the U-shaped voltage dependence of inactivation was more pronounced for heteromeric compared with homomeric channels, and inactivation was shifted to hyperpolarized potentials (Fig. 2 *A–F*). In addition, recovery from inactivation was faster for $_{CFP}$Kv2.1/$_{YFP}$Kv9.3 and $_{YFP}$Kv2.1/$_{CFP}$Kv9.3 channels than for $_{CFP}$Kv2.1 or $_{YFP}$Kv2.1 homomers (Fig. 2 *G* and *H*).

Having established that the tagged Kv2.1 and Kv9.3 subunits reliably reproduce the assembly and function of unmodified α-subunits, we assayed FRET between them (Figs. 3 and 4). When $_{CFP}$Kv2.1 and $_{YFP}$Kv2.1 were coexpressed, both fluorescence signals were limited to the perimeter of the cell (Fig. 3*A*).

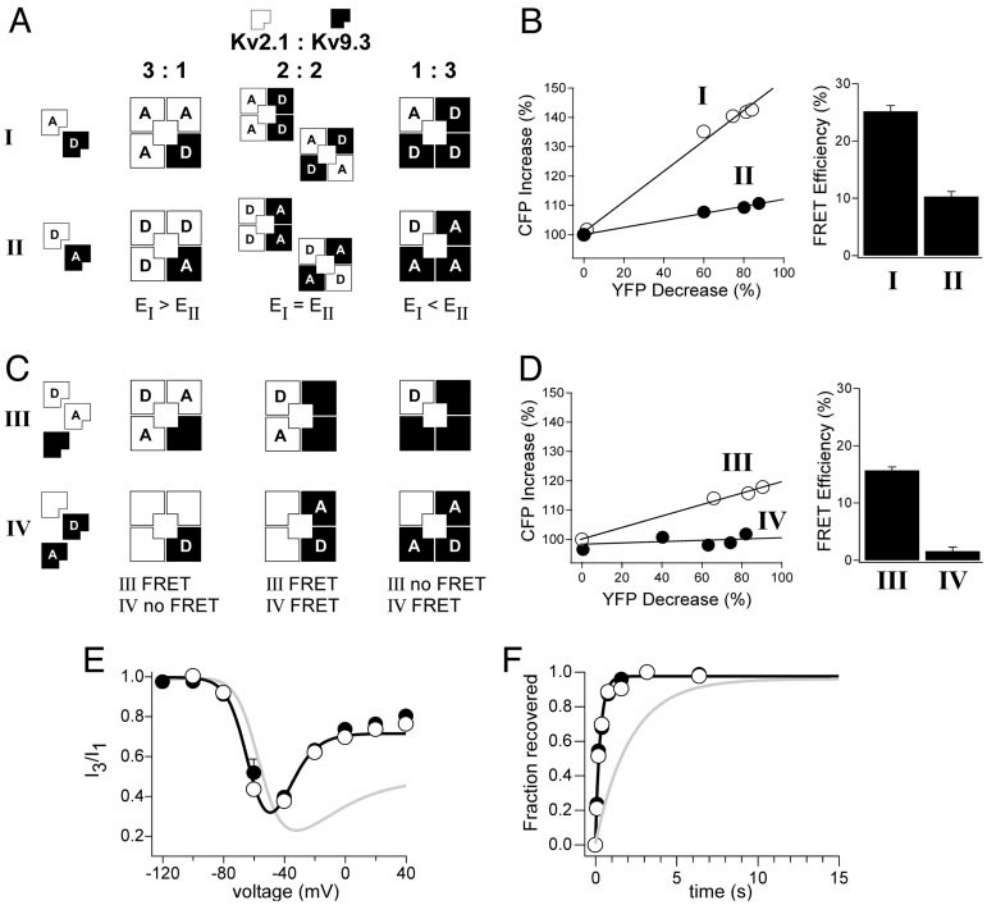


**Fig. 4.** Stoichiometry of heteromeric Kv2.1/Kv9.3 channels. (*A* and *C*) Schematic representation of the experimental paradigms and the resulting relevant subunit assemblies used to determine the stoichiometry of Kv2.1/Kv9.3 channels. Open drawings represent Kv2.1, and filled drawings represent Kv9.3, CFP (D, donor) and YFP (A, acceptor). In the paradigm in *A*, cells were transfected with $_{YFP}$Kv2.1 and $_{CFP}$Kv9.3 (*A*, experiment I) or with $_{CFP}$Kv2.1 and $_{YFP}$Kv9.3 (*A*, experiment II). The relation between the efficiency of energy transfer in these two experiments indicates the stoichiometry of the channels. (*B*) Scatter plots (representative cells) and bar diagrams of FRET efficiencies calculated by using $I_D$ obtained from scatter plots of cells [(*B*, experiment I), $n = 31$; (*B*, experiment II), $n = 14$]. In the paradigm in *C*, cells were transfected with $_{CFP}$Kv2.1, $_{YFP}$Kv2.1 and Kv9.3 (*C*, experiment III) or $_{CFP}$Kv9.3, $_{YFP}$Kv9.3, and Kv2.1 (*C*, experiment IV). In these experiments, the presence or absence of FRET indicates the stoichiometry of the heteromeric channels. Schemes in *C* show the optimal FRET assemblies for each stoichiometry. (*D*) Scatter plots (representative cells) and bar diagrams of FRET efficiencies calculated by using $I_D$ obtained from scatter plots [(*D*, experiment III), $n = 16$; (*D*, experiment IV), $n = 20$]. (*E*) Voltage dependence of inactivation recorded from cells of experiments III (○) and IV (●) as a function of voltage ($n = 6–8$). The results obtained for untagged Kv2.1 (gray line) and Kv2.1/Kv9.3 (black line) channels are shown. (*F*) Representative measurements of recovery from inactivation for experiments III (○) and IV (●). For comparison, least-square fits of monoexponential functions to the data for recovery of untagged Kv2.1 (gray line; $\tau = 2.15$ s) and Kv2.1/Kv9.3 (black line; $\tau = 0.29$ s) channels are shown.

This finding, together with the currents measured in cell-attached patches (data not shown), indicates a predominant localization of the respective channels in the plasma membrane. By contrast, when $_{CFP}$Kv9.3 and $_{YFP}$Kv9.3 were coexpressed, the fluorescence showed a reticular distribution throughout the cell, sparing the nucleus and the plasma membrane (Fig. 3*C*). Throughout this study, FRET was measured by acceptor photobleaching (23). This FRET technique avoids normalization between different cells and allows for quantification of the energy transfer efficiency ($E$). The progress of acceptor photobleaching and concomitant donor dequenching were monitored by repetitive image acquisition and analysis of the relevant region of interest (Fig. 3 *B* and *D*). The increase in CFP intensity, indicating FRET, was plotted against the decrease of YFP intensity, and $I_D$ was extrapolated for complete bleaching of the acceptor. For $_{CFP}$Kv2.1 and $_{YFP}$Kv2.1, FRET was readily detected ($E = 13.3 \pm 0.7\%$, $n = 16$). By contrast, the absence of a FRET signal between $_{CFP}$Kv9.3 and $_{YFP}$Kv9.3 ($E = 1.7 \pm 1\%$, $n = 11$) supports the notion that these modulatory $\alpha$-subunits do not associate in a homomeric fashion *in vivo*, as anticipated by the lack of interaction of their first tetramerization (T1) domains in yeast two-hybrid assays (8, 24). The lack of T1 interaction could inhibit the ER exit of these subunits (Fig. 3*C*) and might serve to assure their targeting to Kv2.1 subunits.

We interpret all FRET signals here to result from the interaction of tagged $\alpha$-subunits within the same channel rather than from adjacent channels for three reasons. First, FRET is limited to fluorophores <10 nm apart, and Kv channels can be approximated as squares that measure ≈10 nm across (25, 26). Second, $E$ did not vary significantly with different YFP or CFP intensities, and thus, was independent of the channel density (27). Third, as reported above (Fig. 3), FRET was observed only between tagged $\alpha$-subunits assembled in one channel but not between subunits merely colocalized.

The inability of Kv9.3 subunits to associate into homomeric channels and the small number of homomeric Kv2.1 channels in cells coexpressing Kv2.1 and Kv9.3 allowed us to study the stoichiometry of heteromeric Kv2.1/Kv9.3 channels in isolation. To this end, we used two independent approaches. The first approach relies on the dependence of $E$ on the donor/acceptor

ratio and the distance between donor and acceptor. Thus, $E$ is higher for a donor that can transfer energy to multiple equidistant acceptors compared with a single acceptor, and $E$ is lower for fluorophores attached to subunits diagonally opposed compared with adjacent subunits (16, 18, 19, 21). The stoichiometry can then be determined by comparing the FRET efficiency from the following two sets of experiments (Fig. 4*A*): (*i*) a series of transfections, where Kv2.1 carries the acceptor (CFP) and Kv9.3 caries the donor (YFP) (Fig. 4*A*, experiment I); and (*ii*) a series of transfections where the Kv2.1 carries the donor and Kv9.3 the acceptor (Fig. 4*A*, experiment II). If the stoichiometry were 2:2, the donor/acceptor ratio and distance would be independent of the subunits to which they are attached, and $E$ should be comparable in both experiments. If heteromeric channels, on the other hand, consisted of one Kv2.1 subunit and three Kv9.3 subunits, then $E$ should be higher when the donor is attached to Kv2.1. Conversely, if channels were composed of three Kv2.1 subunits and one Kv9.3 subunit, $E$ should be higher when the donor is attached to Kv9.3. Indeed, this last case was observed (Fig. 4*B*). When $_{CFP}$Kv2.1 and $_{YFP}$Kv9.3 were coexpressed (Fig. 4*A*, experiment II), $E$ was $10.3 \pm 0.9\%$ ($n = 14$) compared with $25.2 \pm 1.0\%$ ($n = 31$) for coexpression of $_{YFP}$Kv2.1 and $_{CFP}$Kv9.3 (Fig. 4*A*, experiment I). We used these $E$ values and the deduced stoichiometry to estimate the distance between adjacent and diagonally opposed subunits. For coexpression of $_{YFP}$Kv2.1 and $_{CFP}$Kv9.3 (Fig. 4*A*, experiment I), $E$ corresponds to the transfer of energy from the single donor to its two adjacent acceptors. Thus, the distance between adjacent subunits (Eq. **2**) was calculated to be ≈66 Å. Using this value for $R_{adj}$, first $E_{adj}$, and then the distance between subunits across the pore can be calculated (Eq. **3**) for channels formed by $_{CFP}$Kv2.1 and $_{YFP}$Kv9.3 (Fig. 4*A*, experiment II, three donor and one acceptor). This calculation gives a distance between diagonally opposed subunits of ≈93 Å. These results are in striking agreement with the relation of both distances by the Pythagorean theorem (Eq. **4**), which predicts that a square with a side length of 66 Å measures exactly 93 Å across. These findings corroborate the notion that heteromeric channels are indeed tetramers with subunits arranged in a quadratic fashion around the central pore, and correlate well with Kv channel dimensions determined by single-particle EM (26, 28). For the above calculations, we used an $R_0$ value of 49.2 Å (29), which assumes a relative dipole orientation factor $\kappa^2$ of 2/3. This parameter could plausibly vary over some range as could the absolute distances (16). It is important, therefore, to note that our main interest in these calculations was not to measure absolute distances, but rather, to support our interpretation concerning the stoichiometry and geometry of heteromeric channels.

To confirm the stoichiometry of three Kv2.1 subunits and one Kv9.3 subunit per channel, a second approach pioneered by Zheng *et al.* (17) was used, which worked by an all-or-none rule (Fig. 4*C*). Untagged Kv9.3 subunits were coexpressed with $_{CFP}$Kv2.1 and $_{YFP}$Kv2.1. Under these conditions, FRET should only occur if heteromeric channels contained two or more Kv2.1 subunits (Fig. 4*C*, experiment III). In the reverse experiment, fluorophores were attached to Kv9.3 and coexpressed with untagged Kv2.1. FRET was only observed when $_{CFP}$Kv2.1 and $_{YFP}$Kv2.1 were coexpressed with Kv9.3 (Fig. 4 *C*, experiment IV and *D* and $E = 15.7 \pm 0.6\%, n = 16$) but not for the coexpression of Kv2.1 with $_{CFP}$Kv9.3 and $_{YFP}$Kv9.3 (Fig. 4 *C*, experiment IV and *D* and $E = 1.6 \pm 0.7\%, n = 20$), corroborating a stoichiometry of three Kv2.1 and one Kv9.3, and again ruling out significant interchannel FRET. Electrophysiological recordings of the voltage dependence of inactivation (Fig. 4*E*) and recovery from inactivation (Fig. 4*F*) from these cells confirmed the absence of homomeric Kv2.1.

Thus, both independent approaches suggest that heteromeric Kv2.1/Kv9.3 channels associate in a fixed stoichiometry of three Kv2.1 subunits and one Kv9.3 subunit arranged in a square-like fashion around the central pore.

## Discussion

Modulatory α-subunits form the largest group of $K^+$ channel-modifying proteins, comprising one-fourth of all Kv α-subunits (6–12). Here, we report the assembly of the modulatory α-subunit Kv9.3 with Kv2.1 into functional channels consisting of three Kv2.1 subunits and one Kv9.3 subunit. For $K^+$ channels, which have been a beacon of molecular symmetry, this finding stands out from a crowd of heteromeric $K^+$ channels formed by different nonmodulatory α-subunits (30, 31) and assemblies of α-subunit tetramers with transmembrane or intracellular auxiliary proteins reported to result in symmetric complexes with even-numbered stoichiometries (2–5).

The initial phase of tetramerization of Kv channels is guided by an N-terminal recognition domain, referred to as T1 (28, 32). This multipurpose domain, which also serves as a docking station for intracellular auxiliary proteins (3, 5, 33–35) and has been implicated in channel trafficking (36) and gating (14, 15, 37, 38), acts at early stages of assembly when the peptide chains are still attached to ribosomes (39). The function of the T1 domain in the assembly process is 2-fold, providing stabilizing interactions for some, and prohibiting the interaction of other subunits. When the T1 domain is removed, functional channels still form, but specificity of interaction is lost, and the expression level is reduced (40). These and other observations, including the finding that, despite the fourfold symmetry of the T1 domain structure, channel assembly seems to proceed as a dimerization of dimers (41), have led to the conclusion that additional interaction surfaces participate in the assembly of Kv channels. In yeast two-hybrid assays, the T1 domain of modulatory α-subunits was previously shown not to interact in a homomeric fashion, but to selectively interact with the T1 domain of Kv2.1 (8, 24). Additionally, we show here, that full-length Kv9.3 subunits do not associate in a homomeric fashion inside mammalian cells (Fig. 3 *C* and *D*). This finding implies that the formation of dimers of two modulatory α-subunits is very unlikely, whereas heteromeric Kv2.1/Kv9.3 and homomeric Kv2.1 dimers are predicted to form readily. The most parsimonious way then to form a tetrameric channel with three Kv2.1 subunits and one Kv9.3 subunit is to assume that heteromeric dimers can interact with homomeric Kv2.1 dimers, but not among themselves. This could also explain the lower current amplitude consistently observed in mammalian cells and *Xenopus* oocytes coexpressing Kv2.1 and Kv9.3 or other modulatory α-subunits compared with equal amounts of Kv2.1 alone (6, 7, 24), because, as soon as the amount of homomeric Kv2.1 dimers is low, heteromeric dimers would be left without suitable interaction partners.

An alternative mechanism supporting a 3:1 ratio assembly is suggested by analogy with cyclic nucleotide-gated (CNG) channels. CNG channels from rod photoreceptors and olfactory neurons were shown to consist of three CNGA subunits and one CNGB subunit, similar to the Kv2.1/Kv9.3 complexes described here (17, 42, 43). Whereas for CNG channels, considerable evidence for structural and functional organization as dimers of dimers exists (44, 45), a C-terminal leucine zipper domain present in CNGA subunits, but not CNGB subunits, supports a trimeric interaction of CNGA subunits, and thus, favors asymmetric tetramerization (42). At present, no such domain is known for Kv2.1 subunits. However, these subunits have a large C terminus of unknown structure, which could contain additional interaction domains. Defining the protein surfaces that mediate the interaction of Kv2.1 and modulatory α-subunits should help to distinguish between these alternatives and will be an important step toward understanding the mechanisms guiding the specific assembly of Kv2.1/Kv9.3 channels described

here. It remains a striking parallel that for both CNG and Kv channels regulatory principal subunits associate with their targets in a fixed 1:3 ratio stoichiometry.

How relevant is the stoichiometry described here by using a heterologous expression system to the assembly of native channels? Several arguments make us confident that indeed the selective assembly reported here is likely to be found in native channels. First, mRNA and protein expression, biophysical and pharmacological properties, and oxygen sensitivity have allowed for a correlation of Kv2.1/Kv9.3 channels with native channels participating in the hypoxic vasoconstriction of pulmonary arteries (12). Second, expression in *Xenopus* oocytes and mammalian cells by using a range of cRNA and cDNA ratios, respectively, yielded currents with invariant kinetics. The time course of recovery from inactivation and deactivation of these currents is monoexponential, implying that a single population of channels is expressed (9, 12). Third, the notion of a fixed stoichiometry is further supported by the lack of significant variation of the FRET efficiency with various acceptor and donor intensities after coexpression of $_{CFP}$Kv2.1 and $_{YFP}$Kv9.3 or $_{YFP}$Kv2.1 and $_{CFP}$Kv9.3 (16, 27). By analogy, the fixed CNG channel assembly in heterologous systems (17) correlated well with that detected in native channels (42, 43).

Modulatory $\alpha$-subunits influence all gating transitions investigated, with the most striking effects concerning inactivation (7, 9, 10, 13). Thus, Kv9.3 is thought to selectively enhance closed-state inactivation and inhibit open-state inactivation of Kv2.1 (9), conferring to the heteromeric channels unique functional properties, and supporting a distinct role for them in electrical signaling. The mechanism of this inactivation and whether open- and closed-state inactivation occur by the same or different mechanisms is presently unknown. The elucidation of the subunit stoichiometry presented here is a step toward such a mechanistic understanding and allows the conclusion that, similar to C-type (46), the inactivation of Kv2.1 involves a concerted movement of all subunits on which a single modulatory $\alpha$-subunit appears to act as a cooperative effector.

We thank Prof. W. Stühmer for support, equipment, and scientific discussion; Dr. R. E. García-Ferreiro for scientific discussions and assistance with electrophysiology; Dr. G. Bunt (Max-Planck-Institut für Experimentelle Medizin, Göttingen, Germany) for pCB6 plasmids; and Dr. P. Pedarzani for critical reading of the manuscript. This work was supported by a grant from the Wellcome Trust (to M.S.). M.S. is a Wellcome Trust Senior Research Fellow.

1. Hille, B. (2001) *Ion Channels of Excitable Membranes* (Sinauer, Sunderland, MA).
2. Parcej, D. N., Scott, V. E. & Dolly, J. O. (1992) *Biochemistry* **31,** 11084–11088.
3. Gulbis, J. M., Zhou, M., Mann, S. & MacKinnon, R. (2000) *Science* **289,** 123–127.
4. Chen, H., Kim, L. A., Rajan, S., Xu, S. & Goldstein, S. A. (2003) *Neuron* **40,** 15–23.
5. Jerng, H. H., Pfaffinger, P. J. & Covarrubias, M. (2004) *Mol. Cell. Neurosci.* **27,** 343–369.
6. Hugnot, J. P., Salinas, M., Lesage, F., Guillemare, E., de Weille, J., Heurteaux, C., Mattei, M. G. & Lazdunski, M. (1996) *EMBO J.* **15,** 3322–3331.
7. Castellano, A., Chiara, M. D., Mellstrom, B., Molina, A., Monje, F., Naranjo, J. R. & Lopez-Barneo, J. (1997) *J. Neurosci.* **17,** 4652–4661.
8. Post, M. A., Kirsch, G. E. & Brown, A. M. (1996) *FEBS Lett.* **399,** 177–182.
9. Kerschensteiner, D. & Stocker, M. (1999) *Biophys. J.* **77,** 248–257.
10. Salinas, M., Duprat, F., Heurteaux, C., Hugnot, J. P. & Lazdunski, M. (1997) *J. Biol. Chem.* **272,** 24371–24379.
11. Ottschytsch, N., Raes, A., Van Hoorick, D. & Snyders, D. J. (2002) *Proc. Natl. Acad. Sci. USA* **99,** 7986–7991.
12. Patel, A. J., Lazdunski, M. & Honore, E. (1997) *EMBO J.* **16,** 6615–6625.
13. Kramer, J. W., Post, M. A., Brown, A. M. & Kirsch, G. E. (1998) *Am. J. Physiol.* **274,** C1501–C1510.
14. Chiara, M. D., Monje, F., Castellano, A. & Lopez-Barneo, J. (1999) *J. Neurosci.* **19,** 6865–6873.
15. Kerschensteiner, D., Monje, F. & Stocker, M. (2003) *J. Biol. Chem.* **278,** 18154–18161.
16. Lakowicz, J. R. (1999) *Principles of Fluorescence Spectroscopy* (Kluwer, Dordrecht, The Netherlands).
17. Zheng, J., Trudeau, M. C. & Zagotta, W. N. (2002) *Neuron* **36,** 891–896.
18. Mannuzzu, L. M., Moronne, M. M. & Isacoff, E. Y. (1996) *Science* **271,** 213–216.
19. Cha, A., Snyder, G. E., Selvin, P. R. & Bezanilla, F. (1999) *Nature* **402,** 809–813.
20. D'Hoedt, D., Hirzel, K., Pedarzani, P. & Stocker, M. (2004) *J. Biol. Chem.* **279,** 12088–12092.
21. Riven, I., Kalmanzon, E., Segev, L. & Reuveny, E. (2003) *Neuron* **38,** 225–235.
22. Klemic, K. G., Shieh, C. C., Kirsch, G. E. & Jones, S. W. (1998) *Biophys. J.* **74,** 1779–1789.
23. Bastiaens, P. I. & Jovin, T. M. (1996) *Proc. Natl. Acad. Sci. USA* **93,** 8407–8412.
24. Stocker, M., Hellwig, M. & Kerschensteiner, D. (1999) *J. Neurochem.* **72,** 1725–1734.
25. Li, M., Unwin, N., Stauffer, K. A., Jan, Y. N. & Jan, L. Y. (1994) *Curr. Biol.* **4,** 110–115.
26. Sokolova, O., Kolmakova-Partensky, L. & Grigorieff, N. (2001) *Structure (London)* **9,** 215–220.
27. Kenworthy, A. K. & Edidin, M. (1998) *J. Cell Biol.* **142,** 69–84.
28. Li, M., Jan, Y. N. & Jan, L. Y. (1992) *Science* **257,** 1225–1230.
29. Patterson, G. H., Piston, D. W. & Barisas, B. G. (2000) *Anal. Biochem.* **284,** 438–440.
30. Hadley, J. K., Passmore, G. M., Tatulian, L., Al-Qatari, M., Ye, F., Wickenden, A. D. & Brown, D. A. (2003) *J. Neurosci.* **23,** 5012–5019.
31. Silverman, S. K., Lester, H. A. & Dougherty, D. A. (1996) *J. Biol. Chem.* **271,** 30524–30528.
32. Deutsch, C. (2003) *Neuron* **40,** 265–276.
33. Sewing, S., Roeper, J. & Pongs, O. (1996) *Neuron* **16,** 455–463.
34. Yu, W., Xu, J. & Li, M. (1996) *Neuron* **16,** 441–453.
35. An, W. F., Bowlby, M. R., Betty, M., Cao, J., Ling, H. P., Mendoza, G., Hinson, J. W., Mattsson, K. I., Strassle, B. W., Trimmer, J. S. & Rhodes, K. J. (2000) *Nature* **403,** 553–556.
36. Gu, C., Jan, Y. N. & Jan, L. Y. (2003) *Science* **301,** 646–649.
37. Cushman, S. J., Nanao, M. H., Jahng, A. W., DeRubeis, D., Choe, S. & Pfaffinger, P. J. (2000) *Nat. Struct. Biol* **7,** 403–407.
38. Minor, D. L., Lin, Y. F., Mobley, B. C., Avelar, A., Jan, Y. N., Jan, L. Y. & Berger, J. M. (2000) *Cell* **102,** 657–670.
39. Lu, J., Robinson, J. M., Edwards, D. & Deutsch, C. (2001) *Biochemistry* **40,** 10934–10946.
40. Tu, L., Santarelli, V., Sheng, Z., Skach, W., Pain, D. & Deutsch, C. (1996) *J. Biol. Chem.* **271,** 18904–18911.
41. Tu, L. & Deutsch, C. (1999) *Biophys. J.* **76,** 2004–2017.
42. Zhong, H., Molday, L. L., Molday, R. S. & Yau, K. W. (2002) *Nature* **420,** 193–198.
43. Weitz, D., Ficek, N., Kremmer, E., Bauer, P. J. & Kaupp, U. B. (2002) *Neuron* **36,** 881–889.
44. Higgins, M. K., Weitz, D., Warne, T., Schertler, G. F. & Kaupp, U. B. (2002) *EMBO J.* **21,** 2087–2094.
45. Liu, D. T., Tibbs, G. R., Paoletti, P. & Siegelbaum, S. A. (1998) *Neuron* **21,** 235–248.
46. Yellen, G. (1998) *Q. Rev. Biophys.* **31,** 239–295.